J Solid State Electrochem (2011) 15:503–510
DOI 10.1007/s10008-010-1122-9

ORIGINAL PAPER

Improvement in stability of $LiMn_2O_4$ thin-film electrodes by oxygen-plasma irradiation to precursor gel

Yoshiaki Matsuo · Yosohiro Sugie · Kouta Sakamoto · Tomokazu Fukutsuka

Received: 18 April 2010 / Revised: 23 May 2010 / Accepted: 31 May 2010 / Published online: 9 June 2010

Abstract $LiMn_2O_4$ thin-film electrodes were prepared by the sol–gel method combined with oxygen-plasma irradiation. Oxygen plasma with a power of 10 or 90 W was irradiated to the precursor thin film prepared from lithium acetate, manganese acetate tetrahydrate and polyvinylpyrrolidone on a Pt plate, and then it was fired at 723 or 973 K. X-ray diffraction and Raman measurements indicated that oxygen-plasma irradiation was effective to increase the crystallinity of the resulting $LiMn_2O_4$. Atomic force microscope observation showed that the particle size of $LiMn_2O_4$ in the resulting thin-film electrode was decreased and homogeneous distribution of $LiMn_2O_4$ particles was achieved. Oxidation of the electrolyte at higher potentials was suppressed and capacity retention at 328 K was dramatically improved for the $LiMn_2O_4$ thin-film electrode obtained at 973 K. The improved electrochemical stability is ascribed to the elimination of organic materials from precursor by oxygen-plasma irradiation.

Keywords Lithium-ion battery · Lithium manganese oxide · Oxygen plasma · Stability

Y. Matsuo (✉) · Y. Sugie · K. Sakamoto
Graduate School of Engineering, University of Hyogo,
2167 Shosha,
Himeji, Hyogo 671-2280, Japan
e-mail: ymatsuo@eng.u-hyogo.ac.jp

T. Fukutsuka
Graduate School of Engineering, Kyoto University,
Nishikyo-ku,
Kyoto 615-8510, Japan
e-mail: fuku@elech.kuic.kyoto-u.ac.jp

Introduction

Spinel-type lithium manganese oxide ($LiMn_2O_4$) is one of the most attractive active materials as a positive electrode for lithium ion batteries, because of its low cost, high capacity, low toxicity, and so on. $LiMn_2O_4$ is usually obtained by a solid-state reaction at high temperatures ranging from 923 to 1023 K [1]. However, low-temperature syntheses are desired for mass production and energy conservation. Solution-based methods (sol–gel method [2], Pechini process [3], co-precipitation [4], etc.) have been investigated as methods for the low-temperature synthesis of $LiMn_2O_4$. These solution-based methods give $LiMn_2O_4$ with a fine particle size, a narrow particle size distribution, and uniform composition, which provide high electrochemical performance, that is, enhancement of effective reaction areas or high power use. In the solution-based methods, the precursors usually contain organic materials to maintain the Li–Mn–O framework. These organic materials must be eliminated from the precursors by relatively high-temperature firing to obtain $LiMn_2O_4$. High-temperature firing promotes the growth of particles. Moreover, heat of combustion generated by the firing of carbon atoms in organic materials leads to the growth of particles. Therefore, organic materials must be eliminated by some other process to obtain finer $LiMn_2O_4$ particle from solution-based methods.

In our previous letter, we have shown that oxygen-plasma irradiation was effective to decrease the particle size of $LiMn_2O_4$ [5]. Oxygen plasma contains active oxygen species such as O^{2-}, $O\cdot$, O^{+}, O_2^{-}, and O^{2+}. Some of these active species are strong oxidants, and can oxidize organic components of the precursor. When the organic components are removed from precursor before firing, the heat generated by the combustion of organic components during

firing should be decreased. This can avoid the growth of $LiMn_2O_4$ crystalline. In addition to this, we have also found that the oxidative current at high potentials decreased when the sample was treated by oxygen-plasma irradiation. It has been reported by many researchers that $LiMn_2O_4$ electrodes suffer from the capacity fading especially at elevated temperatures [6–10]. The above phenomena suggests that the dissolution of manganese ions from $LiMn_2O_4$ are suppressed in spite of the increased surface area and the suppression of capacity fading is expected even when the $LiMn_2O_4$ electrodes prepared with oxygen plasma treatment are cycled at elevated temperatures.

In this paper, therefore, we prepared $LiMn_2O_4$ thin-film electrodes from the precursor gel thin films modified by the oxygen-plasma irradiation. Effects of the oxygen-plasma irradiation on the electrochemical properties of $LiMn_2O_4$ thin-film electrode were discussed. In particular, the improvement in the stability of a $LiMn_2O_4$ thin-film electrode at an elevated temperature was found.

Experimental

Precursor gel was prepared by a sol–gel method using polyvinylpyrrolidone (PVP) as reported by Kanamura et al. [11], since the sol and the gel obtained by this method is very stable. Lithium acetate (CH_3COOLi; Wako Pure Chemical) was selected as a lithium source and manganese acetate tetrahydrate ($Mn(CH_3COO)_2{\cdot}4H_2O$; Wako Pure Chemical) as a manganese source. Solvents were ethanol, water, and acetic acid. The molecular weight of PVP (Aldrich) as a stabilizer was 55,000. Li–Mn–O sol was spin-coated onto a Pt sheet and dried at 393 K to obtain a precursor gel thin film. Spin-coating was carried out once at 3,000 rpm. The precursor thin film was introduced into the plasma irradiation chamber. The detail of procedure was described previously [5, 12]. Oxygen-plasma irradiation was carried out for 1 h. Plasma was generated by an rf power supply at 13.56 MHz, and the applied rf power was set at 10 or 90 W. The flow rate of oxygen and argon was set at 50 and 25 dm^3 min^{-1}, respectively, and the total pressure in the chamber was kept at 66 Pa. Modified precursor thin film was fired at 723 or 973 K for 2 h in air using an electric furnace, and $LiMn_2O_4$ thin-film electrode was obtained. Hereafter, the $LiMn_2O_4$ thin-film electrode obtained by the above process is referred to as $LiMn_2O_4$-xW-yK (x is an applied rf power, and y is a firing temperature). For example, $LiMn_2O_4$ thin-film electrode obtained by firing at 723 K from precursor thin film modified by oxygen-plasma irradiation at 10 W is referred to as $LiMn_2O_4$–10 W–723 K. For comparison, unmodified precursor thin film was also fired at the same temperatures. Hereafter, the $LiMn_2O_4$ thin-film electrode obtained by the above process is referred to as $LiMn_2O_4$-zK (z is a firing temperature).

X-ray diffraction (XRD; Rint-2100) and Raman spectroscopy (Jobin-Yvon; T-64000) were used to characterize the resulting thin films. Typical working conditions for XRD were 30 kV and 30 mA, with a scanning speed of 2° min^{-1}. Raman measurements were carried out at 298 K using a spectrometer equipped with micro-optics. A 514.5-nm line from an Ar^+ laser was used, and the power of the incident laser light was maintained at 10 mW. Atomic force microscope (AFM) observation was carried out using Nanopics1000 to evaluate the particle size of the resulting thin films. Cyclic voltammetry (CV) and electrochemical impedance spectroscopy (EIS) are performed as electrochemical measurements using a three-electrode cell. A $LiMn_2O_4$ thin-film electrode was used as a working electrode. Lithium metal was used as both counter and reference electrodes. Electrolytes consisting of PC containing 1 mol dm^{-3} $LiClO_4$ were used. CV was conducted at room temperature and 328 K by using HSV-100F (HOKUTO-DENKO Inc.). The scanning range was between the immersion potential and 4.4 V (vs. Li/Li^+). Sweep rate at room temperature and 328 K was 0.1 and 1 mV/s, respectively. EIS was conducted by using Sorlatron 1260 impedance gain-phase analyzer and Sorlatron 1286 electrochemical interface in a frequency range of 100 kHz–10 mHz at various electrode potentials by using ZPlot 2 program. Measurement was carried out with an ac amplitude 5 mV. All experiments were conducted under an Ar atmosphere. Unless otherwise stated, the potential is referenced to against Li/Li^+.

Results and discussion

Crystallinity of $LiMn_2O_4$ thin-film electrodes

Figure 1 shows the XRD patterns of $LiMn_2O_4$ thin film obtained at (a) 723 and (b) 973 K. The diffraction peak observed at about 2θ=24° is due to the adhesive tape. In Fig.1a, the diffraction peaks were observed at about 2θ= 19° and 36.5° corresponding to the (111) and (311) planes for all the samples, indicating the formation of spinel-$LiMn_2O_4$ [13]. There was no major difference among $LiMn_2O_4$-723 K, $LiMn_2O_4$-10 W-723 K, and $LiMn_2O_4$-90 W-723 K in their peak positions. This result shows that the lattice parameter was almost unchanged. And the calculated crystallite sizes from Scherrer's equation using the full-widths at half-maximum of the (111) line are 18 and 19 nm for $LiMn_2O_4$-723 K and $LiMn_2O_4$-10 W-723 K, respectively. The FWHM of $LiMn_2O_4$-90 W-723 K could not be estimated due to the disturbance of background peak. Hence, it was found that crystallinity of bulk was not

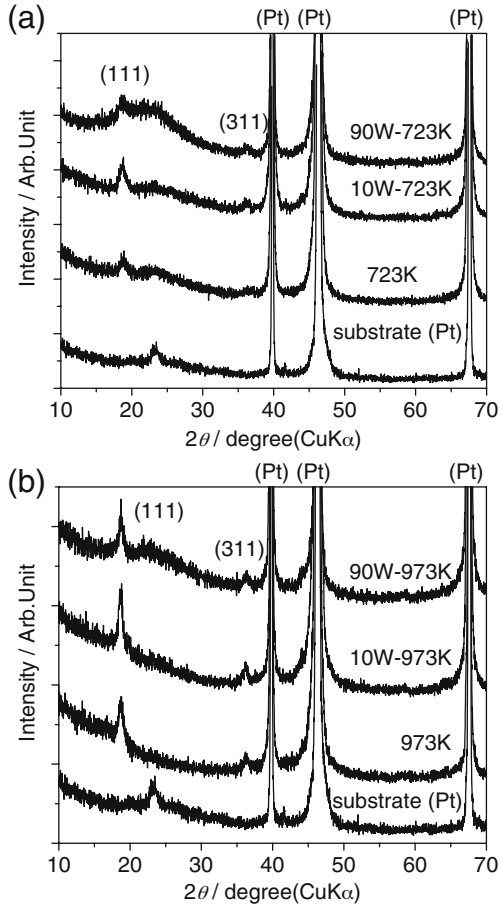

Fig. 1 X-ray diffraction patterns of resulting $LiMn_2O_4$ thin films. **a** $LiMn_2O_4$ thin films obtained at 723 K, **b** $LiMn_2O_4$ thin films obtained at 973 K. *Numbers* on peaks denote index hkl

changed by the oxygen-plasma irradiation. As shown in Fig. 1b, when the thin film sample was fired at 923 K, the calculated crystallite sizes from Scherrer's equation are 22 nm for $LiMn_2O_4$-973 K, and 26 nm for $LiMn_2O_4$-10 W-973 K, and 24 nm for $LiMn_2O_4$-90 W-973 K. This result also indicates that the crystallinity of $LiMn_2O_4$ phase was not affected by oxygen-plasma irradiation, as was observed for the sample prepared at 723 K. Next, surface crystallinity was examined by Raman spectroscopy. Micro-Raman spectroscopy was used to characterize the resulting thin films. Figure 2 shows the Raman spectra of $LiMn_2O_4$ thin film obtained at (a) 723 and (b) 973 K. In Fig. 2a, broad peaks appeared at around 640 cm^{-1}. The peak at around 640 cm^{-1} can be divided into two peaks at around 630 and 650 cm^{-1}. The peak at around 630 cm^{-1} is assigned to the symmetric A_{1g} mode of the $LiMn_2O_4$ spinel phase [14]. The peak at around 650 cm^{-1} would be due to the existence of some manganese oxide (Mn_xO_y) phase [15, 16]. Since the XRD patterns did not show any peaks due to Mn_xO_y (33° for Mn_2O_3 and 36° for Mn_3O_4), we could not determine the chemical formula of this manganese oxide species. Fig. 2b shows the Raman spectra of $LiMn_2O_4$ thin film obtained at 973 K. At this temperature, a peak assigned to the A_{1g} mode was clearly observed at around 630 cm^{-1} for both $LiMn_2O_4$-10 W-973 K and $LiMn_2O_4$-90 W-723 K and the peak at around 650 cm^{-1} was not observed in all thin films. This is due to the relatively high-temperature firing. This result shows that surface crystallinity was enhanced by oxygen-plasma irradiation.

Surface morphology of $LiMn_2O_4$ thin-film electrodes

AFM observation was conducted to clarify the influence of oxygen-plasma irradiation on the size and distribution of particles. Figure 3a–c show AFM images of $LiMn_2O_4$ thin film obtained at 723 K. In Fig. 3a, chain-like structures

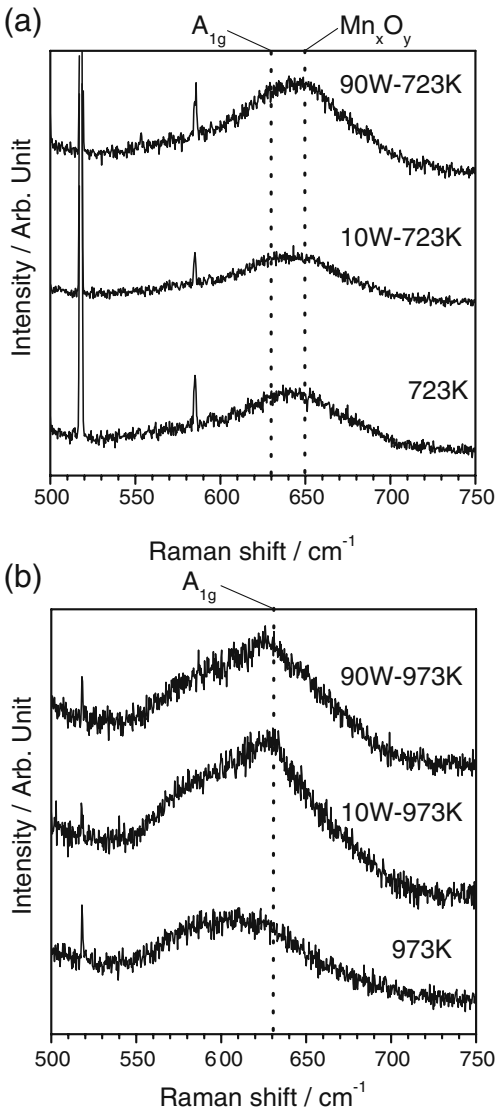

Fig. 2 Raman spectra of resulting $LiMn_2O_4$ thin films. **a** $LiMn_2O_4$ thin films obtained at 723 K, and **b** $LiMn_2O_4$ thin films obtained at 973 K

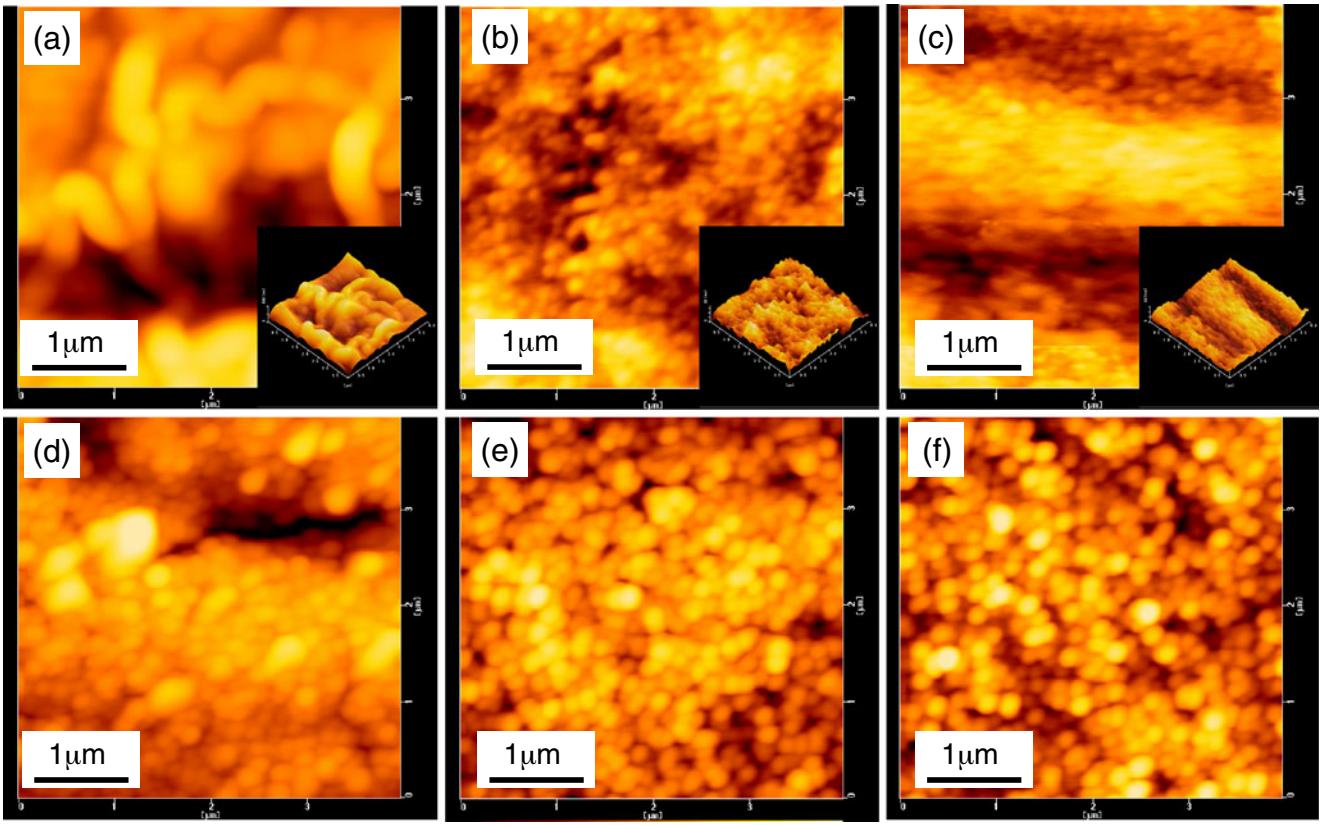

Fig. 3 AFM images of resulting $LiMn_2O_4$ thin films. (**a**–**c**) $LiMn_2O_4$ thin films obtained at 723 K, and (**d**–**f**) $LiMn_2O_4$ thin films obtained at 973 K

consisting of large particles were observed as the surface morphology of $LiMn_2O_4$-723 K. In contrast, the particle sizes of both $LiMn_2O_4$-10 W-723 K and $LiMn_2O_4$-90 W-723 K were much smaller and the distribution of particle size was homogeneous as shown in Fig. 3b and c. However, difference of applied rf power did not influence the morphology. This result indicated that applied rf power of 10 W was enough to modify the surface of the precursor. Figure 3d–f show AFM images of $LiMn_2O_4$ thin film obtained at 973 K. Unlike with the result obtained for the film prepared at 723 K, the particle size of both $LiMn_2O_4$-10 W-973 K and $LiMn_2O_4$-90 W-973 K was almost identical to that of $LiMn_2O_4$-973 K. However, particles were more homogeneously distributed when oxygen-plasma was irradiated. In general, the particle sizes of ceramic materials are dependent on the firing temperature. However, the particle size of $LiMn_2O_4$-10 W-723 K and $LiMn_2O_4$-90 W-723 K is much smaller than that of $LiMn_2O_4$-723 K. This result suggests that active oxygen species generated by oxygen-plasma irradiation eliminated the organic materials from precursor and suppressed the growth of $LiMn_2O_4$ particles at a lower firing temperature (723 K). On the other hand, at a higher temperature (973 K), the thermal energy given from outside was so large that the particle size of the resulting $LiMn_2O_4$ was not apparently affected by the reduction of heat from the combustion of organic materials by oxygen-plasma irradiation. However, homogeneous distribution of particles was achieved at a relatively high firing temperature (973 K). This could be ascribed to the homogenous heating of the sample during firing realized by the elimination of organic materials by oxygen-plasma irradiation to the precursor. At a higher temperature (1073 K), both particle size and distribution of particles were not influenced by oxygen-plasma irradiation due to the large thermal energy supplied from outside. Based on these results, it was clarified that firing temperature of 973 K gives the good surface morphology by oxygen-plasma irradiation.

Electrochemical properties of $LiMn_2O_4$ thin-film electrodes at room temperature

Lithium ion extraction/insertion behavior of the $LiMn_2O_4$ thin-film electrodes was examined by cyclic voltammetry at room temperature. Figure 4 shows CVs at the first cycle of $LiMn_2O_4$ thin-film electrodes obtained at 723 K. As shown in Fig. 4, $LiMn_2O_4$ thin-film electrodes show two pairs of redox peaks at around 4.00 and 4.15 V as reported in the literature [17]. For $LiMn_2O_4$-723 K(a) and $LiMn_2O_4$-90 W-723 K(c), two oxidative peaks were not clearly separated.

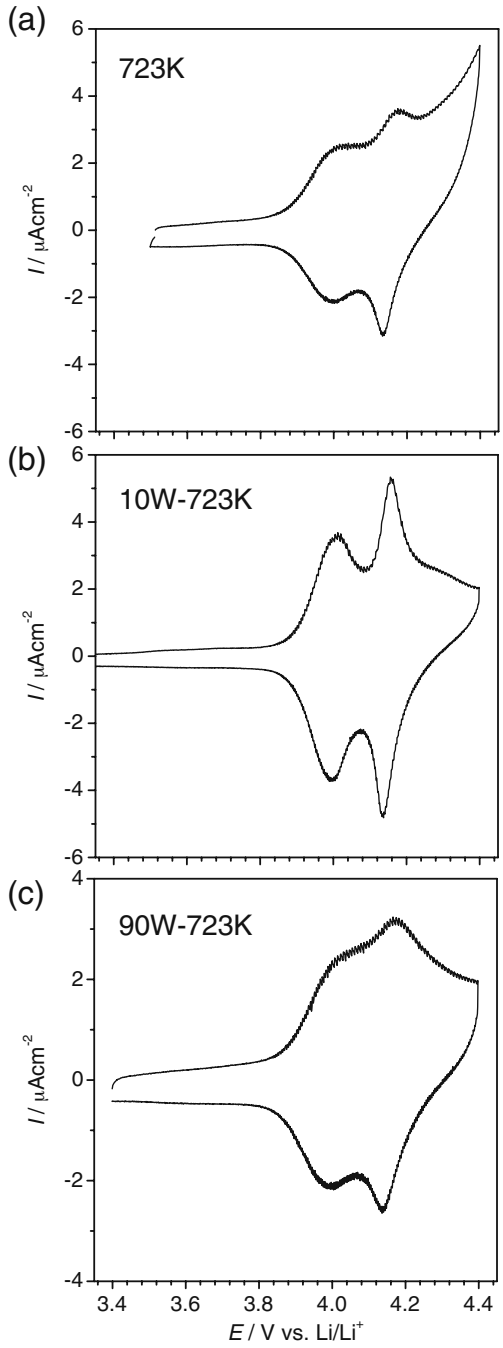

Fig. 4 CVs (1st cycle) of $LiMn_2O_4$ thin-film electrodes obtained at 723 K in 1 mol dm^{-3} $LiClO_4$/PC at room temperature. Scanning rate is 0.1 mV/s. **a** Without oxygen-plasma irradiation, **b** with oxygen-plasma irradiation at 10 W, and **c** with oxygen-plasma irradiation at 90 W

By contrast, two oxidative peaks were clearly separated for $LiMn_2O_4$-10 W-723 K(b). This is due to the decrease of particle size of $LiMn_2O_4$ by oxygen-plasma irradiation at 10 W which facilitated the insertion/extraction of lithium ions into/from $LiMn_2O_4$, since decrease of particle size deliver the decrease of lithium ion diffusion length within particle and the reduction of charge-transfer resistance which are the origin of internal resistance for insertion/extraction of lithium ions. On the other hand, the oxidative currents at 4.4 V of $LiMn_2O_4$-10 W-723 K(b) and $LiMn_2O_4$-90 W-723 K(c) were much smaller than that of $LiMn_2O_4$-723 K(a). From Raman spectra shown in Fig.2, it is assumed that Mn_xO_y existed at the surface of $LiMn_2O_4$-10 W-723 K and $LiMn_2O_4$-90 W-723 K. Active oxygen species generated in oxygen-plasma oxidized not only organic materials but also cation such as Li in the precursor, and therefore, lithium deficiencies were formed on the surface of precursor and quite thin Mn_xO_y layer might be formed after firing. So far, various surface coatings of $LiMn_2O_4$ by metal oxide and improvement of electrochemical properties have been reported [18–24]. Hence, this thin Mn_xO_y layer would also act as buffer layer between $LiMn_2O_4$ and electrolyte, and oxidative currents at 4.4 V decreased. In addition, the reason why the lithium ion extraction/insertion peaks were not clearly separated for $LiMn_2O_4$-90 W-723 K could be because the cations in the precursor was excessively oxidized by the irradiation of oxygen-plasma at a high rf power. Similar tendency was observed for $LiMn_2O_4$ thin-film electrodes obtained at 973 K. Figure 5 shows CVs at the first cycle of $LiMn_2O_4$ thin-film electrodes obtained at 973 K. In Fig. 5, $LiMn_2O_4$-10 W-973 K showed better electrochemical property. It is found that oxygen-plasma irradiation at 10 W was effective to enhance the CV behavior of $LiMn_2O_4$ thin-film electrodes.

Next, the variation of charge-transfer resistance by oxygen-plasma irradiation at 10 W was examined by EIS measurement. Figure 6 shows Nyquist plot of $LiMn_2O_4$-723 K and $LiMn_2O_4$-10 W-723 K(a), and $LiMn_2O_4$-973 K and $LiMn_2O_4$-10 W-973 K(b) at 4.00 V. The values of charge-transfer resistances of $LiMn_2O_4$ thin-film electrode with oxygen-plasma irradiation were smaller than those of $LiMn_2O_4$ thin-film electrode without oxygen-plasma irradiation. Taking into account for the results of XRD measurements and AFM observations, this result would be due to the increase of the crystallinity and the reaction area by oxygen-plasma irradiation at 10 W. Based on the above results, it was revealed that oxygen-plasma irradiation at 10 W improved the electrochemical properties of $LiMn_2O_4$ thin-film electrode. Hence, stability of $LiMn_2O_4$ at high temperature was examined for the $LiMn_2O_4$ thin-film electrodes with oxygen-plasma irradiation at 10 W.

Electrochemical properties of $LiMn_2O_4$ thin-film electrodes at 328 K

Figure 7 shows high-temperature (328 K) CVs (first and 50th cycle) of $LiMn_2O_4$ thin-film electrodes obtained at 723 K and 973 K. It was found that the decrease of peak-current after cycling was more gradual for the $LiMn_2O_4$

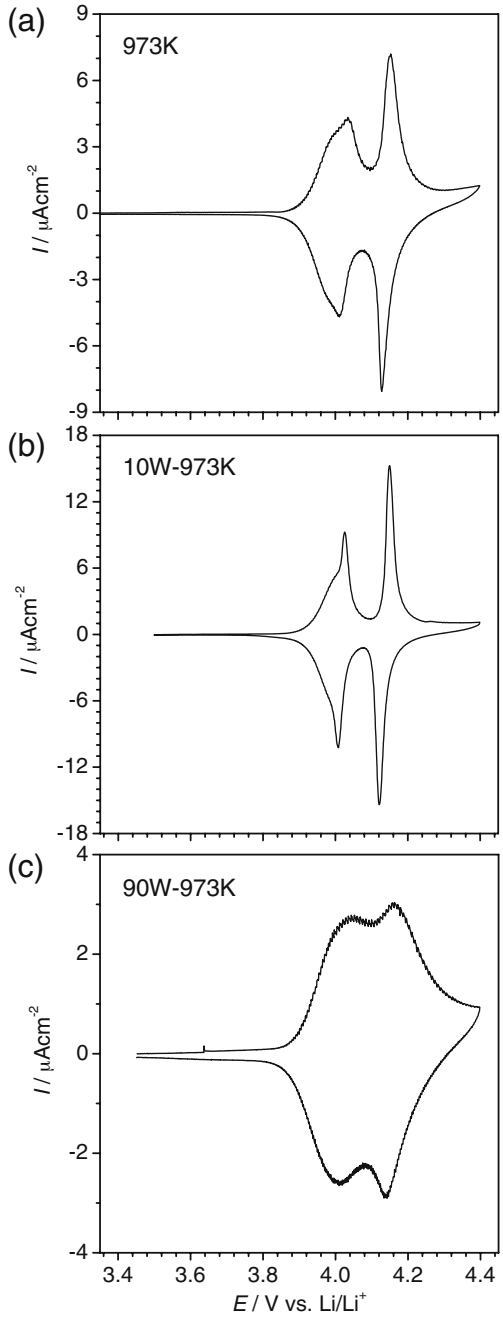

Fig. 5 CVs (1st cycle) of $LiMn_2O_4$ thin-film electrodes obtained at 973 K in 1 mol dm^{-3} $LiClO_4$/PC at room temperature. Scanning rate is 0.1 mV/s. **a** Without oxygen-plasma irradiation, **b** with oxygen-plasma irradiation at 10 W, and **c** with oxygen-plasma irradiation at 90 W

thin-film electrodes with oxygen-plasma irradiation at both firing temperatures. To make this result understandable, the variation of capacity retention rate obtained from CV is shown in Fig. 8. Each capacity was normalized by the capacity at the 1st cycle. Capacity retention rates of $LiMn_2O_4$-723 K and $LiMn_2O_4$-10 W-723 K after the 50th cycle were almost identical. By contrast, the capacity retention rate of $LiMn_2O_4$-10 W-973 K after the 50th cycle was higher than that of $LiMn_2O_4$-973 K. Oxygen-plasma irradiation leads to the enhancement of the crystallinity and increase of the active surface area as discussed in the previous section. Although the enhancement of the crystallinity brings to the improvement of stability at high temperatures [25], capacity retention rate of $LiMn_2O_4$-723 K was almost identical to that of $LiMn_2O_4$-973 K. Based on this result, the crystallinity enhancement by oxygen-plasma irradiation is not the main reason for the improved stability of $LiMn_2O_4$ electrodes in this study. Increase of the active surface area is not also suitable for the reason of deteriorated capacity retention rate, since the enhancement of $LiMn_2O_4$/electrolyte interface should lead to the increase of the dissolution of manganese ion. Chen et al. reported that α-MnO_2-modification of $LiMn_2O_4$ lead the improvement in thermal stability due to the protection of the framework of $LiMn_2O_4$ by α-MnO_2 sheathes [19]. In the previous section, Mn_xO_y was observed in Raman spectra for $LiMn_2O_4$-10 W-723 K. Although there is no

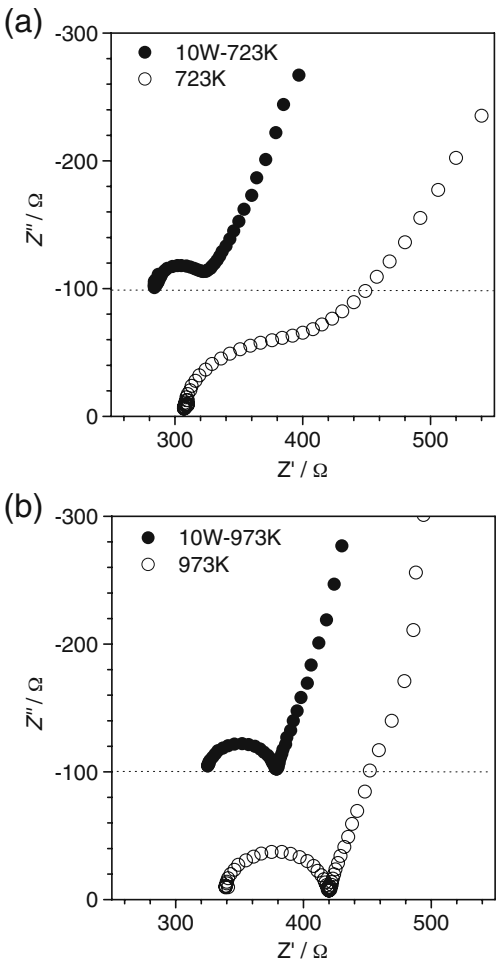

Fig. 6 Nyquist plots of $LiMn_2O_4$ thin-film electrodes obtained at 723 K (**a**) and 973 K (**b**) in 1 mol dm-3 LiClO4/PC at room temperature. Nyquist plots were measured at 4.00 V

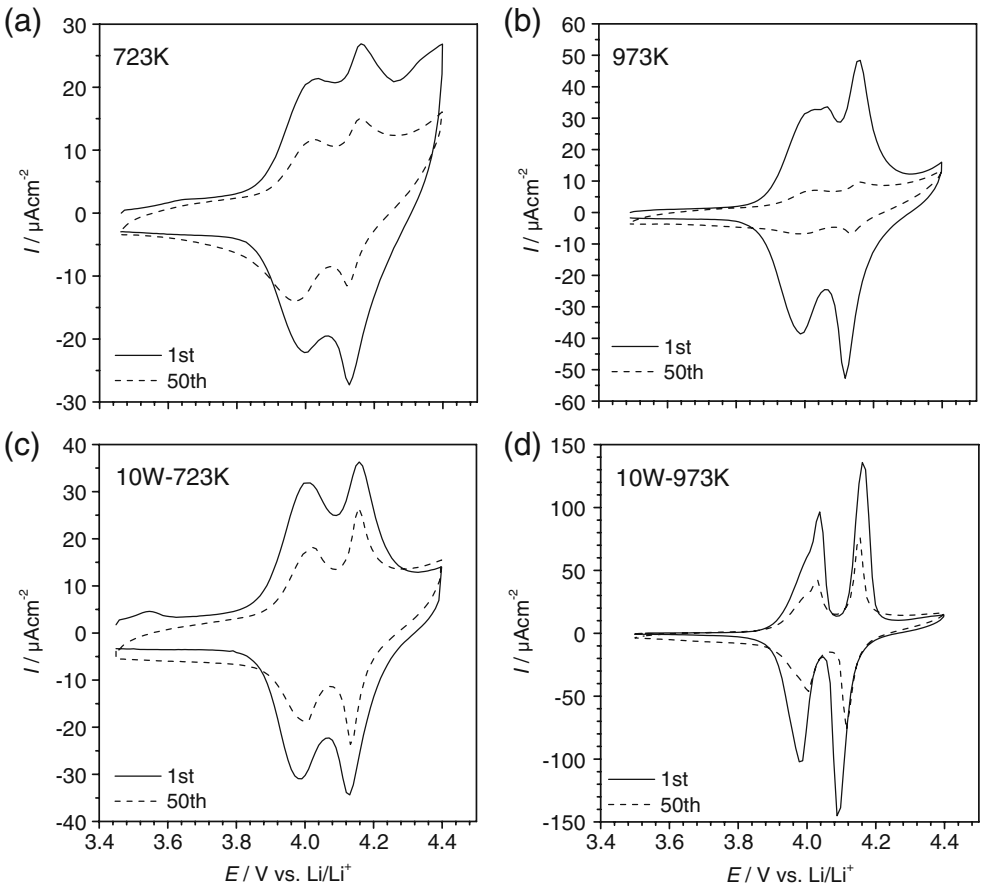

Fig. 7 CVs of $LiMn_2O_4$ thin-film electrodes obtained at 723 K (**a** and **b**), $LiMn_2O_4$ thin films obtained at 973 K (**c** and **d**) in 1 mol dm^{-3} $LiClO_4$/PC at 328 K. Scanning rate is 1 mV/s

clear evidence of the formation of manganese oxides for $LiMn_2O_4$-10 W-973 K, thin layer of manganese oxide, such as α-MnO_2, should be formed by the lithium deficit due to the oxidation by oxygen plasma. Hence, we should take into account the manganese oxide as the buffer layer between $LiMn_2O_4$ and electrolyte. This is probably the reason of both suppression of oxidative decomposition of electrolyte and improvement in the stability at high-temperature cycling. As a conclusion, oxygen-plasma irradiation that can bring various advantages to $LiMn_2O_4$ would be useful method to prepare $LiMn_2O_4$.

Conclusion

$LiMn_2O_4$ thin-film electrodes were prepared by the sol–gel method combined with oxygen-plasma irradiation. XRD measurement revealed that the lattice parameter and the size of crystallite were almost unchanged by the oxygen-plasma irradiation. Raman spectroscopy revealed that surface crystallinity was enhanced by the oxygen-plasma irradiation and manganese oxide layer existed of at surface. The particle size of the resulting $LiMn_2O_4$ thin-film electrode obtained at 723 K became small and homogeneous distribution of particles was achieved by oxygen-plasma irradiation. For the $LiMn_2O_4$ thin-film electrode obtained at 973 K, particle size was not changed dramatically, but particles were more homogeneously distributed. This might be due to the influence of the elimination of organic materials from precursor. The electrochemical properties of the resulting $LiMn_2O_4$ thin-film electrode were summarized as follows: (1) quick response of lithium ion extraction/

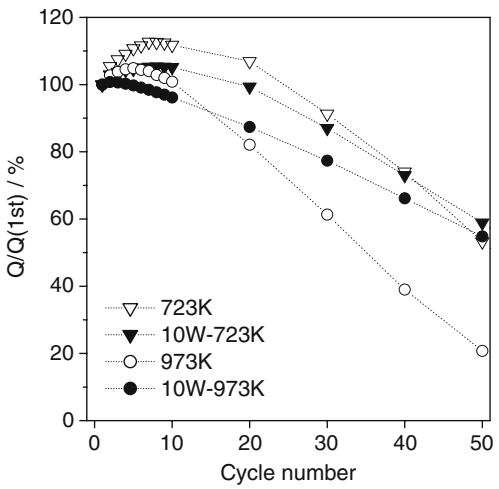

Fig. 8 Capacity retention obtained from CVs in Fig. 7. Each capacity was normalized by the capacity of the first cycle

insertion, (2) suppression of oxidative decomposition of electrolyte solution, and (3) improved high-temperature cycling stability. As a conclusion, it is considered that oxygen-plasma irradiation is quite attractive method to give $LiMn_2O_4$ thin-film electrodes various advantages at once.

References

1. Tarascon JM, Wang E, Shokoohi FK, McKinnon WR, Colson S (1991) J Electrochem Soc 138:2859–2864
2. Bach S, Henry M, Baffier N, Livage J (1990) J Solid State Chem 88:325–333
3. Liu W, Farrington GC, Chaput F, Dunn B (1996) J Electrochem Soc 143:879–884
4. Barboux P, Tarascon JM, Shokoohi FK (1991) J Solid State Chem 94:185–196
5. Fukutsuka T, Sakamoto K, Matsuo Y, Sugie Y, Abe T, Ogumi Z (2004) Electrochem Solid-State Lett 7:A481–A483
6. Thackeray MM (1997) Prog Solid State Chem 25:1–71
7. Arora P, White RE, Doyle M (1998) J Electrochem Soc 145:3647–3667
8. Amatucci G, Pasquier AD, Blyr A, Zhang T, Tarascon JM (1999) Electrochem Acta 45:255–271
9. Gummow RJ, Kock A, Thackeray MM (1994) Solid State Ion 69:59–67
10. Jang DH, Shin J, Oh SM (1996) J Electrochem Soc 143:2204–2211
11. Rho YH, Kanamura K, Umegaki T (2003) J Electrochem Soc 150: A107–A111
12. Fukutsuka T, Hasegawa S, Katayama T, Matsuo Y, Sugie Y, Abe T, Ogumi Z (2003) Electrochem 71:1111–1113
13. Inaba M, Doi T, Iriyama Y, Abe T, Ogumi Z (1999) J Power Sources 81(82):554–557
14. Ammundsen B, Burns GR, Islam MS, Kanoh H, Rozière J (1999) J Phys Chem 103:5175–5180
15. Matsuo Y, Kostecki R, MacLarnon F (2001) J Electrochem Soc 148:A687–A692
16. Bernard MC, Goff AHL, Thi BV, Torresi SC (1993) J Electrochem Soc 140:3065–3070
17. Yamada I, Abe T, Iriyama Y, Ogumi Z (2003) Electrochem Commun 5:502–505
18. Kannan AM, Manthiram A (2002) Electrochem Solid State Lett 5: A167–A169
19. Chen GS, Chen GS, Hsiao HH, Louh RF, Humphreys CJ (2004) Electrochem Solid-State Lett 7:A235–A238
20. Sun Y, Wang Z, Chen L, Huang X (2003) J Electrochem Soc 150: A1294–A1298
21. Liu H, Cheng C, Zongqiuhu, Zhang K (2007) Mater Chem Phys 101:276–279
22. Chan HW, Duh JG, Lee JF (2006) Electrochem Commun 8:1731–1736
23. Li C, Zhang HP, Fu LJ, Liu H, Wu YP, Rahm E, Holze R, Wu HQ (2006) Electrochim Acta 51:3872–3883
24. Gnanaraj JS, Pol VG, Gedanken A, Aurbach D (2003) Electrochem Commun 5:940–945
25. Amatucci GG, Pereira N, Zheng T, Tarascon JM (2001) J Electrochem Soc 148:A171–A182